IChemE

0957–5820/99/$10.00+0.00

Trans IChemE, Vol 77, Part B, January 1999

AN ASSESSMENT OF THE CONTAINMENT PERFORMANCE OF A VENTILATED ENCLOSURE IN THE PHARMACEUTICALS INDUSTRY USING EXPERIMENTAL AND PREDICTIVE TECHNIQUES

J. M. REGLAR, G. L. QUARINI, M. J. TIERNEY (MEMBER) and M. P. ANDERSON*

Department of Mechanical Engineering, University of Bristol, Bristol, UK
**Zeneca Pharmaceuticals, Avlon Works, Bristol, UK*

Due to guidelines issued by government health bodies, concerns over personnel safety, and a desire to maintain the quality of manufactured products, containment is becoming increasingly important in a growing number of different industrial contexts. By isolating hazardous materials, a containment system should reduce to acceptably low levels the potential dangers posed to human health and the surrounding environment. During manufacturing processes, it should also assist in the protection of these materials from outside contamination.

In this paper, a ventilated containment booth at a pharmaceuticals plant is analysed. This booth is used to contain active powders whilst they are tipped into a reactor for drug manufacture. Experimental data regarding the air flows within the system is compared with numerical predictions generated using computational fluid dynamics (CFD). The agreement is good and the predictions highlight the flow dynamics of the system. The use of CFD is then extended to provide indicators of containment performance for a range of different operational characteristics. These indicators, based on the ventilation performance of the system, and on the ability of the air flow at the hatch face to isolate hazardous materials from the working environment, clearly show the deficiencies associated with the current system. However, they also indicate that certain modifications to the location of the extraction ducting and the rate of air extraction could yield substantial benefits in terms of the overall containment performance of the device.

Keywords: containment; solids charging isolator; CFD; face velocity; fluid age; indicators of performance.

INTRODUCTION

Containment is the process whereby material is held within defined boundaries and isolated from regions where its presence is unwanted. Applications of containment are widespread, particularly within the nuclear, pharmaceutical and food industries, and usually involve segregating hazardous materials and directing them into areas where they can no longer contaminate human resources, pollute working environments or spoil manufactured products.

The methods of containing a contaminant source zone may be termed either 'passive' or 'active' control measures[1]. Passive measures, such as those followed in order to isolate contaminated soils, involve the construction of physical barriers that should be either completely impermeable or reduce to acceptably low levels the potential for advective and diffusive transport of contaminants into 'clean' locations.

Active measures are generally concerned with the use of air flows to regulate and control hazardous materials. Flow is usually provided by either dilution ventilation which removes small quantities of contaminants released into the workroom, or by local exhaust ventilation which contains toxic substances at their source. Alternatively, displacement ventilation may be employed. This method 'flushes out' contaminants by introducing air at one location and extracting from an opposite location[2]. Quarini *et al.*[3], for example, studied the hydrodynamic performance of clean rooms. These rooms use dilution ventilation in order to remove minute particulates from the air space and prevent them from contaminating intricate electronic components. Similar rooms, which house specifically designed laminar biological safety cabinets with airlocks and computer-controlled pressure systems, are used in biotechnology environments. Here the aim is to contain, remove and eventually kill potentially dangerous organisms leaking from bioprocesses such as cell propagation and inoculum preparation[4,5].

In the pharmaceuticals industry, a range of various passive or active control measures are presently employed depending on the potency and quantity of the hazardous material concerned, and the intended operation[6]. For highly

toxic materials and research compounds, an isolator is used to provide 'barrier containment' (passive measure) corresponding to a maximum operator exposure limit (OEL) of $< 1\,\mu g\,m^{-3}$. 'Airflow containment' (active measure) is normally used for OELs of between $10\,\mu g\,m^{-3}$ and $10{,}000\,\mu g\,m^{-3}$. Within this range, downflow booths with workstations are employed for the containment of ethical pharmaceuticals, while a local exhaust hood is thought adequate for the control of excipient products[7]. The more effective the device is in terms of protecting the operator, the greater is the capital investment required.

This work concentrates on the use of local exhaust ventilation as a facility for containment in the pharmaceuticals industry. The particular apparatus analysed, a 'solids charging isolator', is used to isolate toxic materials during the charging process that precedes drug manufacture. Being an airflow containment system, this device is not suitable for any applications requiring an OEL of $< 10\,\mu g\,m^{-3}$. The aim of this system is to distance the raw materials from the surrounding working environment. The extract system is employed to capture and remove any fraction of the inventory remaining in the isolator air space following the charging procedure.

The focus of this work is quite unusual, particularly due to the complex topology of the isolator and the relatively high Reynolds numbers generated within the enclosure. However, similar studies of weaker flows within more simple geometries have been undertaken on fume cupboards which are used extensively in the chemical industries to isolate toxic substances during chemical processes. Hu *et al.*[8], for example, investigated the effects of various factors on the leakage of contaminant from a fume cupboard. They found that marked improvements in containment could be achieved by repositioning the outlet at the rear of the booth, and hence reducing recirculation near to the inlet door. Similarly, Özdemir *et al.*[9] analysed the containment performance of a fume cupboard concentrating primarily on how the geometry of the cabinet influences the flow structures within it. They concluded that the spanwise vortex created close to the upper frontal part of the enclosure can destabilize the inflowing air stream along the sash handle and lead to severe leakage of contaminants trapped within the vortex itself.

Two methods have been used to investigate the operational characteristics of a solids charging isolator at a Zeneca Pharmaceuticals Plant in Avonmouth, Bristol. Firstly, the air flow distributions both within the ventilated enclosure and at the hatch face have been measured *in situ*. Secondly, computational fluid dynamics (CFD) has been applied to the apparatus. Having been used extensively in the nuclear, automobile, aircraft and oil and gas industries in particular, CFD is now encompassing activities concerned with food, pharmaceuticals and bioprocesses. Agutter *et al.*[10], for example, used CFD to predict the tracks followed by micro-organisms from their most likely point of release in a bioprocess, and estimate the number which might be collected from different sampling points within the processing area.

In addition, an attempt has been made to evaluate the performance of this containment system by focusing on two of its more important characteristics. Firstly, the nature of the air flows at the hatch face separating the toxic materials from the operators in the surrounding room has been analysed. A guideline issued by the Health and Safety Executive (HSE)[11] recommends a minimum hatch face velocity of $0.5\,m\,s^{-1}$ for this type of apparatus. Secondly, since it is vital that any residual particulate material with the potential to migrate out into the room or collect on exposed surfaces is extracted as quickly as possible, a performance assessment based on ventilation efficiency has also been carried out. Many studies of ventilation efficiency have been undertaken[12,13,14]. However, few have utilized the predictive advantage of CFD and little has been done to investigate how to optimize air flows within complex geometries.

Experimental and computational data have been compared and the predictive abilities of CFD have been used to investigate how the alterations of certain key operational characteristics of the system are likely to influence its overall containment performance.

THE SOLIDS CHARGING ISOLATOR

The charging isolator contains hazardous pharmaceuticals whilst they are being charged (tipped) into a reactor below. Figure 1 shows the isolator, which has a total height (y) of 2.78 m, total width (x) of 1.04 m and total breadth (z) of 1.04 m. The isolator has a circular hatch face of 0.88 m diameter and four glove ports of 0.3 m diameter to facilitate handling of the material liner by the operator. The circular hatch is positioned on the front face which is at an angle θ of 60 degrees to the horizontal xz-plane. Air is drawn out of the enclosure via a small outlet of area $0.028\,m^2$ using a 4 KW extraction fan driving two such systems. Within the main body of the isolator, there is an inner hopper that converges lower down into a rectangular chute leading into the reactor. This inner hopper supports a grid (0.76 m square) onto which the liner of charging material is initially placed. The region between the inner hopper and the outer hopper (exterior surface) of the isolator is called the rim vent.

The principle of operation is relatively simple. Through use of a mechanically driven drum tipper, a drum of volume $0.2\,m^3$ containing a liner full of the charging material (~ 100 kg of material) is raised and rotated until the top of the drum is positioned at the entrance to the hatch face of the isolator. With the drum held in this inclined position, the liner is allowed to fall into the isolator and onto the supporting grid. Then, using a knife, the operator cuts open this liner via the glove ports and, in so doing, releases the material. At the time of release, the drum tipper has been removed, and the hatch face is completely open to the external environment.

The bulk of the material falls under gravity through the inner hopper to be processed. However, operators have observed that a small proportion of the particulates remain in the isolator air space following the charging procedure. Extracting air from the enclosure has the effect of lowering the internal air pressure and hence hopefully ensuring that no hazardous material leaks out of the hatch face into the working environment. Residual particulates captured by the extraction mechanism pass through cylindrical ductwork to be collected on a large high efficiency particulate air (HEPA) filter.

The rate of air extraction is normally $0.46\,kg\,s^{-1}$ ($1656\,kg\,hr^{-1}$) and, as illustrated in Figure 1, the extract duct is located on one corner of the isolator at a height of

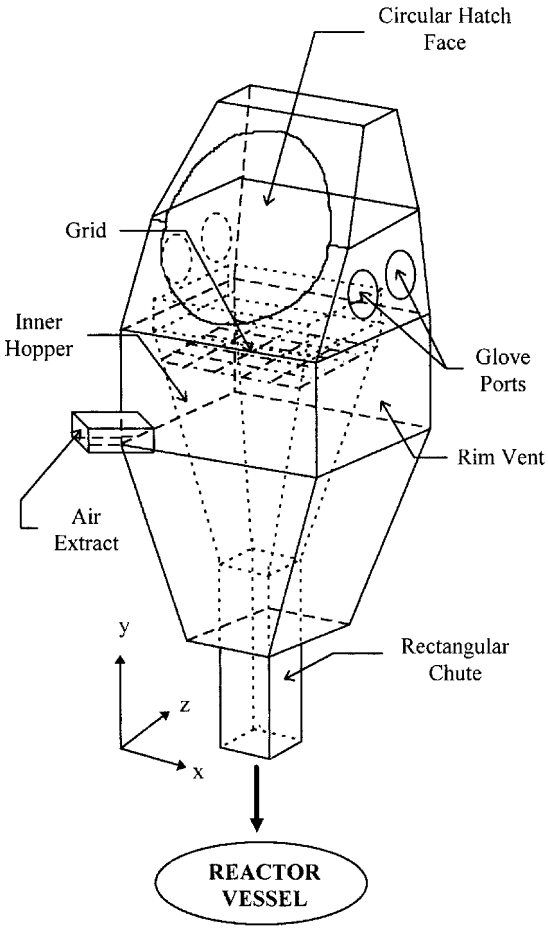

Figure 1. Schematic of the solids charging isolator.

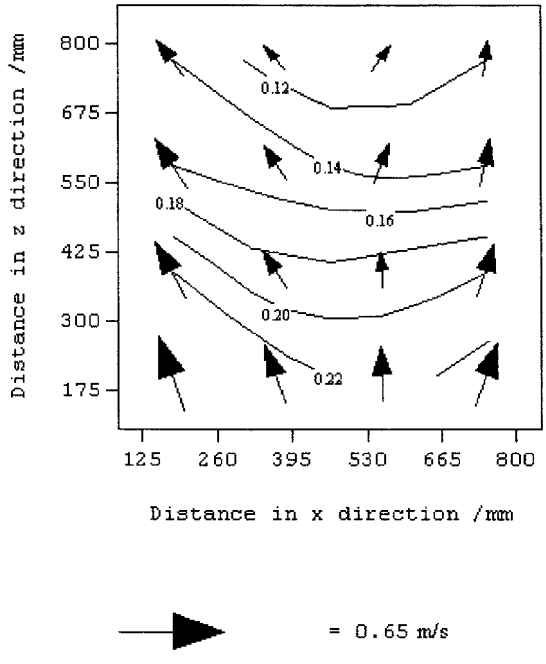

Figure 2. Vector plot of the *u* and *w* components of the measured air speed over a contour plot of the v velocity, on the *xz*-plane at $y = 2.16$ m.

approximately 1.4 m from its base. The clean, filtered air travels out of the plant where it is released into the atmosphere.

EXPERIMENTAL WORK

Introduction

Air flows in the charging isolator were measured for two reasons. Firstly, the nature of the flow field within the isolator air space and the magnitudes of the containing flows at the hatch face were investigated in order to understand how the system functions and obtain indications of its containment efficiency.

Given that the extent of on-site experimental work was constrained by safety regulations and tight manufacturing schedules, CFD was proposed as the method for analysing different operational scenarios. Hence secondly, *in-situ* measurements were taken in order that a comparison could be made with the numerical data, and a certain degree of confidence could be established in the predictive approach.

Procedure

With air being extracted at $0.46\,\mathrm{kg\,s^{-1}}$, the three component velocities of the air flow were measured both within the isolator and at the hatch face using a thermal anemometer with a reported precision of $0.05\,\mathrm{m\,s^{-1}}$. Each reading was averaged over a 20 second time interval and each set of results was repeated twice.

Results

Figure 2 shows the air flow field recorded on the *xz*-plane at a vertical height of 0.42 m from the grid ($y = 2.16$ m). The tendency for the air to move from the hatch face towards the rear of the isolator whilst being influenced by the strong suctions developed in the side vents (between the inner and outer hoppers of the isolator) is clearly evident. The contours show the distribution of the v component of the air speed. This component is always in the negative *y* direction, and is strongest near to the hatch face of the isolator.

Figure 3 shows a contour plot of the w-velocity (velocity in the *z* direction) at the circular hatch face of the isolator. This highlights the strong inward flows of about $2.0\,\mathrm{m\,s^{-1}}$ generated close to the base of the face. Further up the face,

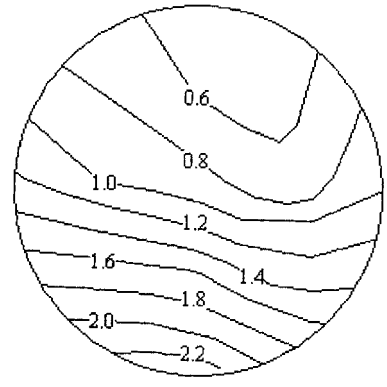

Figure 3. Contour plot of the measured *w*-velocity at the hatch face.

these flows gradually reduce and a region of particularly low velocity was found towards the top right section of the hatch face. However, reasonably high inflows (~ 0.8 $m\,s^{-1}$) were measured near to the edge of the hatch over the majority of its circumference. There was no evidence of any back flow out of the hatch face.

NUMERICAL MODELLING

Computational Grid and Physical Boundaries

A commercial CFD code, CFX 4.2 produced by AEA Technology, was used to model the operational characteristics of the isolator. Due to the relatively complex geometry of the isolator, a total of 114 blocks of cells were required in order to replicate accurately the exterior topology, inner hopper, and extraction position of the system. A mesh consisting of a total of 95,140 computational grid cells was generated and this is shown in Figure 4. The average cell volume is 1.8×10^{-5} m^3 and the average cell orthogonality is 12.5°, where the orthogonality is the maximum deviation from 90° of any pair of adjacent edges meeting at a vertex.

The open circular hatch face through which air enters the enclosure was modelled through use of a series of pressure boundaries on the three blocks constituting the slanting front surface. These pressure boundaries fix the pressure at the face, and correct the velocity distribution whilst applying the condition of mass flow continuity. Thus, at the hatch face, the conditions satisfied are:

$$P = \text{constant} \tag{1}$$

and

$$\frac{\partial u}{\partial x} + \frac{\partial v}{\partial y} + \frac{\partial w}{\partial z} = 0 \tag{2}$$

In (2), the rate of change of density with time is ignored since the flow was assumed to be incompressible. A pressure boundary was also set at the base of the rectangular chute that leads into the reactor vessel, where the nature of the air flow into the isolator was unknown.

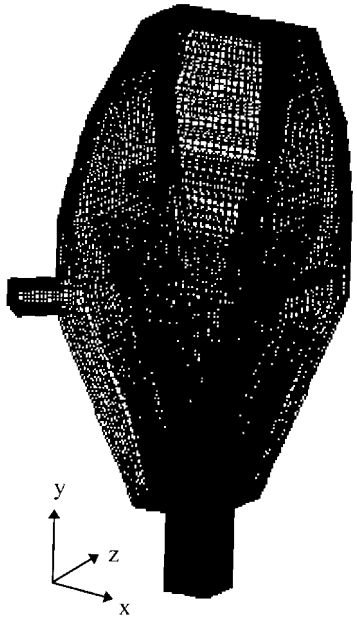

Figure 4. CFD mesh for the solids charging isolator.

The appropriate extraction mass flow rate of 0.46 $kg\,s^{-1}$ was generated by imposing a mass flow boundary condition at the outlet register, which has a modelled area of 0.0266 m^2. Where a mass flow boundary is used for a single outlet, all transported quantities except for velocity are given zero normal gradient. Velocity is given a constant normal gradient across the boundary. This is equivalent to an assumption of fully developed flow and, as such, it is most accurate to position the boundary downstream of the important flow domain, i.e. at the end of a section of ducting as was done in this case.

Solution Equations and Turbulence Models

The standard *k*-epsilon turbulence model was employed in order to simulate the turbulent flows within the isolator air space. This model uses an eddy viscosity hypothesis and assumes that the Reynolds stresses occurring in the turbulent flows may be linearly related to the mean velocity gradients in a manner analogous to the relationship between the stress and strain tensors in laminar Newtonian flow[15].

The continuity and momentum equations solved in the computational domains for the *k*-ε model are:
Continuity equation:

$$\frac{\partial \rho}{\partial t} + \nabla(\rho U) = 0 \tag{3}$$

Momentum equation:

$$\frac{\partial \rho U}{\partial t} + \nabla(\rho U \otimes U) - \nabla(\mu_{eff} \nabla U) = -\nabla P + \rho g \tag{4}$$

$$\text{where } \mu_{eff} = \mu + \mu_T \tag{5}$$

and

$$\mu_T = C_\mu \frac{\rho k^2}{\varepsilon} \tag{6}$$

By introducing a general variable φ, equation (4) may be summarized by the scalar advection-diffusion transport equation:

$$\frac{\partial \rho \varphi}{\partial t} + \nabla(\rho U \varphi - \Gamma \nabla \varphi) = S \tag{7}$$

where Γ is the diffusion coefficient and *S* is a source or sink term representing the creation or destruction of φ.

The scalar transport equations for *k* and epsilon are:

$$\frac{\partial \rho k}{\partial t} + \nabla(\rho k U) = \nabla\left[\frac{\mu_T}{\sigma_k} \nabla k\right] + 2\mu_T E_{ij}.E_{ij} - \rho\varepsilon \tag{8}$$

$$\frac{\partial (\rho\varepsilon)}{\partial t} + \nabla(\rho \varepsilon U) = \nabla\left[\frac{\mu_T}{\sigma_e} \nabla \varepsilon\right] + C_{1e}\frac{\varepsilon}{k} 2\mu_T E_{ij}.E_{ij} - C_{2\varepsilon}\rho\frac{\varepsilon^2}{k} \tag{9}$$

The equations comprise five adjustable constants: C_μ, σ_k, σ_ε, $C_{1\varepsilon}$, $C_{2\varepsilon}$. For the standard *k*-epsilon model, the values of these constants are: $C_\mu = 0.09$; $\sigma_k = 1.00$; $\sigma_\varepsilon = 1.30$; $C_{1\varepsilon} = 1.44$; $C_{2\varepsilon} = 1.92$, and were derived from a process of data fitting to a wide range of turbulent flows[15]. The Prantl numbers σ_k and σ_ε connect the diffusivities of *k* and ε to the eddy viscosity μ_T. E_{ij} is a matrix that describes the mean rate of deformation of a fluid element in a turbulent flow.

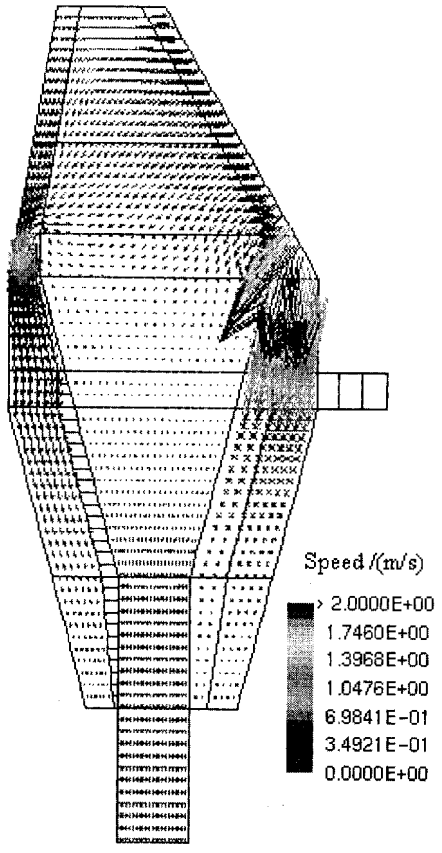

Figure 5. Vector plot of air speed on the *yz*-plane at $x = 0.52$ m.

Solution Procedure

The CFD code discretizes these complex non linear equations using a standard hybrid differencing scheme[16]. The resulting algebraic expressions are then linearized by the Rhie-Chow interpolation technique[17,18]. The SIMPLEC algorithm[19] is used as the basis for updating pressure and correcting velocity components for continuity.

It was found that 800 iterations and false time steps (FTS) of 1×10^{-4} s on the three component velocities and the turbulence quantities were sufficient in order to produce an adequately converged solution (the ratio of the mass residuals from the second and last iterations was 1.1×10^{5}). Where an FTS value is used, the equations are modified in the same way as if each outer iteration is a time step, with two differences: the 'old' time values used are the most recently calculated values of each of the variables; and the time increment may be chosen arbitrarily to achieve the best convergence rate[15].

A vector plot of air speed on the *yz*-plane at $x = 0.52$ m is shown in Figure 5. Figure 6 shows a CFD prediction for the flow field on the *xz*-plane at $y = 2.16$ m whilst Figure 7 shows the computational data concerning the *w*-velocity at the hatch face. These may be compared with Figures 2 and 3 respectfully.

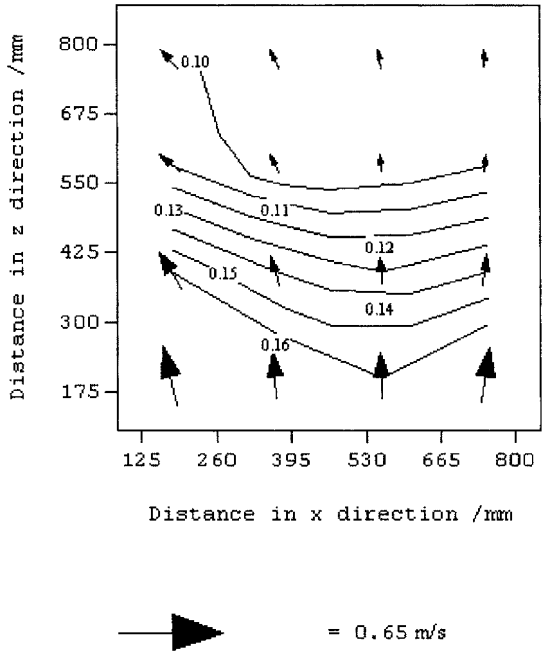

Figure 6. Vector plot of the *u* and *w* components of the predicted air speed over a contour plot of the v velocity, on the *xz*-plane at $y = 2.16$ m.

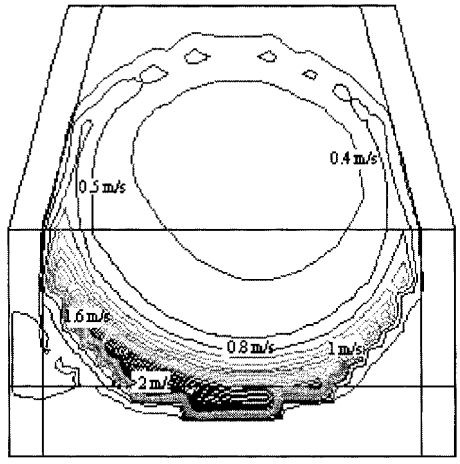

Figure 7. Contour plot of the predicted *w*-velocity at the hatch face.

Grid Independence

Generally, since the discretization process is applied at grid nodes, a finer mesh leads to a more accurate solution, provided convergence is adequate. However, the finer the grid, the greater the solution cost in terms of required computer hardware and calculation time. Where similar convergence statistics and final solutions can be proved to be found through use of a coarser mesh, grid independence has been shown and this smaller mesh is sufficient for accurate results[20].

In this work, grid sizes of 66,562 cells, 95,140 cells and 152,296 cells have been used to solve for one particular model. For all three meshes, the ratio of the mass residual from the second and last iterations was of the order of 1.0×10^{5}. Hence it was assumed that the solution had converged sufficiently. The results produced at three identical positions for each simulation are shown in Table 1. Since, on average, the largest deviation from the mean value for each set of corresponding velocity components is just 4.31%, it is evident that the dependence of the solution on grid size is satisfactory for engineering purposes.

Table 1. Grid independence: the data produced for three different grid sizes.

Co-ordinate position	Velocity component	Number of grid cells used in model			Mean Value of component	Maximum % deviation from mean
		66562	95140	152296		
$x = 0.500$	u	–3.42E–02	–3.43E–02	–3.45E–02	–3.43E–02	0.58
$y = 2.175$	v	–1.01E–01	–8.94E–02	–9.00E–02	–9.35E–02	8.02
$z = 0.564$	w	1.10E–01	1.18E–01	1.18E–01	1.15E–01	4.35
$x = 0.500$	u	–1.83E–02	–1.94E–02	–1.94E–02	–1.90E–02	3.68
$y = 2.347$	v	–1.03E–01	–9.94E–02	–9.74E–02	–9.99E–02	2.50
$z = 0.602$	w	1.10E–01	1.22E–01	1.19E–01	1.17E–01	4.27
$x = 0.502$	u	–1.28E–02	–1.48E–02	–1.28E–02	1.35E–02	9.63
$y = 2.486$	v	–7.58E–02	–7.78E–02	–7.72E–02	–7.69E–02	1.40
$z = 0.632$	w	1.15E–01	1.18E–01	1.09E–01	1.14E–01	4.39
					Average	4.31%

Performance Indicators

The images generated by the post processing facilities of the CFD code provide a good, global picture of the air movements generated in the isolator. However, it is difficult to gain from these images a true picture of containment performance. With this in mind, two performance indicators have been developed enabling the effects of different operational characteristics on containment ability to be compared more quickly.

Evaluation of isolation performance

The degree to which the containment system isolates the surrounding environment from contamination is dependent upon the nature of the protective air flow at the hatch face. We define an Indicator of Isolation Performance (IOIP) according to the HSE guideline recommending a minimum face velocity of 0.5 $\mathrm{m\,s^{-1}}$ for containment. This face velocity, V_n, is defined as the air velocity component normal to the hatch face. The co-ordinate transformation study for this case is given by:

$$\begin{bmatrix} V_N \\ V_{P1} \\ V_{P2} \end{bmatrix} = \begin{bmatrix} 0 & -\cos\theta & \sin\theta \\ 0 & \sin\theta & \cos\theta \\ 1 & 0 & 0 \end{bmatrix} \begin{bmatrix} u \\ \mathrm{v} \\ w \end{bmatrix} \tag{10}$$

where θ is the angle of the hatch face to the horizontal xz-plane.

Hence, the face velocity is deduced from:

$$V_N = w\sin\theta - \mathrm{v}\cos\theta \tag{11}$$

The code within the CFD framework has been modified to compute this value over the whole hatch face area during the solution procedure. Then, the IOIP value has been generated whereby this coefficient represents the proportion of the hatch face area where the face velocity is ≥ 0.5 $\mathrm{m\,s^{-1}}$. Hence, perfect isolation according to this indicator is only achieved by an IOIP value of unity.

Evaluation of ventilation performance

Ventilation performance relates to the efficiency with which residual particulates in the isolator air space are removed into the extract system. If zones within the isolator are not effectively ventilated, then particles are likely to deposit on surfaces in these areas. This not only poses a serious health hazard but also increases the need for regular cleaning of the isolator.

One way of analysing the effectiveness of a ventilation system is by using the concept of 'fluid age'. This is set to zero as a fluid particle enters a ventilated enclosure but increases as the particle is advected through the enclosure towards the outlet. Regardless of any maldistributions in the flow, the mean fluid age at the outlet position (mean residence time of the air), t_o, is always equal to the nominal time constant of the ventilating system (mean turnover time), τ[21].

Hence:

$$\tau = \frac{V}{\dot{V}} = t_o \tag{12}$$

For a perfect 'piston' flow system, whereby fluid elements entering the enclosure at the same instant in time move through it with constant and equal velocity on parallel paths, it is possible to show that the mean fluid age within the system, t_m, is equal to one half of the mean fluid age at the outlet[12,13]. In practise, however, this ideal ventilating system is never realized. Outside the principal flow stream, there are stagnation or re-circulation zones where the air volume is not being efficiently 'flushed' through the system. Here, the fluid will reside for longer periods of time and become 'older'. Hence in 'real' ventilation systems, the mean fluid age is always greater than half the outlet fluid age. Therefore, to summarize:

$$t_m \geq \tfrac{1}{2}\, t_o \tag{13}$$

Fluid age may be computed in CFD by modifying the scalar advection-diffusion transport equation.

Expanding equation (7) gives the three-dimensional transport equation:

$$\rho\left(\frac{\partial\varphi}{\partial t} + u\frac{\partial\varphi}{\partial x} + \mathrm{v}\frac{\partial\varphi}{dy} + w\frac{\partial\varphi}{\partial z}\right) - \left(\frac{\partial}{\partial x}\Gamma_x\frac{\partial\varphi}{\partial x} + \frac{\partial}{\partial y}\Gamma_y\frac{\partial\varphi}{\partial y} + \frac{\partial}{\partial z}\Gamma_z\frac{\partial\varphi}{\partial z}\right) = S \tag{14}$$

For a steady state problem, $\frac{\partial}{\partial t} \rightarrow 0$ and, assuming zero diffusion, $\Gamma_x = \Gamma_y = \Gamma_z \rightarrow 0$. Hence:

$$\rho\left(u\frac{\partial\varphi}{\partial x} + \mathrm{v}\frac{\partial\varphi}{\partial y} + w\frac{\partial\varphi}{\partial z}\right) = S \tag{15}$$

If the passive scalar is taken to be the age of fluid denoted t_a, then this equation becomes:

$$\rho\left(u\frac{\partial t_a}{\partial x} + \mathrm{v}\frac{\partial t_a}{\partial y} + w\frac{\partial t_a}{\partial z}\right) = S \tag{16}$$

At the inlet register $\varphi = t_a = 0$ and at the outlet register $(\partial\varphi/\partial n) = (\partial t_a/\partial n) = 0$.

At all other boundaries $\varphi = \mathrm{t_a} = 0$.

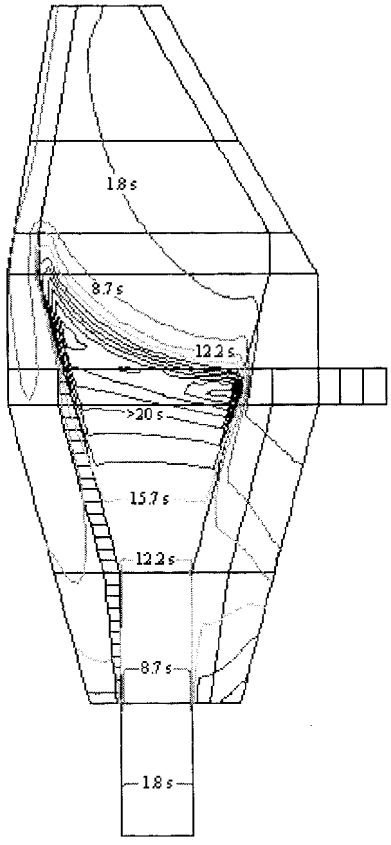

Figure 8. Contour plot of fluid age on the *yz*-plane at $x = 0.52$ m.

In order to maintain dimensional continuity, the source term is set equal to the density ρ to give:

$$\rho\left(u\frac{\partial t_a}{\partial x} + v\frac{\partial t_a}{\partial y} + w\frac{\partial t_a}{\partial z}\right) = \rho \tag{17}$$

In principal, the age of the fluid within a recirculation zone where the fluid is completely 'trapped' should be infinity. However, this limiting condition will never be predicted correctly. Although the diffusivity terms (Γ_x, Γ_y and Γ_z) have been set to zero, there will nonetheless be some numerical diffusion.

Solution of equation (17) throughout the computational domain of the isolator has given the distribution of fluid age within the isolator. Figure 8 presents a contour plot of fluid age on the *yz*-plane at $x = 0.52$ m.

The volume averaged mean fluid age of the whole system, t_m, has been calculated and an Indicator of Ventilation Performance (IOVP) for the isolator has been developed whereby IOVP relates this average 'age' to the 'age' at outlet t_o, i.e.:

$$\text{IOVP} = \frac{1}{2}\left(\frac{t_o}{t_m}\right) \tag{18}$$

Perfect ventilation, such as that produced in the piston flow situation, is indicated when IOVP = 1.

Analysis of Specific Zones within the Isolator

In addition, in order to gain a greater understanding of how the whole containment system functions in terms of ventilation, volume-averaged fluid age calculations have been undertaken for specific zones within the isolator (Figure 1):

- Ventilated Zone—the region that is most effectively ventilated. Consists of the outer hopper of the system including the rim vents.
- Lower Rim Vents—the region in which particulate matter is likely to collect. Consists of the rim vents below the extract position.
- Inner Hopper—consists of the inner hopper of the system through which the charging material falls into the reactor below.
- Proposed Ventilated Zone—the region analysed since it could lead to a direct design improvement for future systems. Consists of the ventilated zone excluding the poorly ventilated lower rim vents.

Scenarios Simulated

To identify designs that might lead to improved efficiency, CFD calculations were carried out for various flow rates and two further extraction positions as highlighted in Figure 9. For all the simulations, the area of the extraction ducting was maintained at approximately $0.028\,\text{m}^2$. However, for extraction position 3, the air was drawn from the isolator into the ducting through an area of $0.076\,\text{m}^2$.

The decision regarding turbulence model depended on the Reynolds number at the hatch face denoted Re_f. If the characteristic length scale is taken as the hatch face diameter, this dimensionless number is given by:

$$Re_f = \frac{\rho \bar{V}_N d_f}{\mu} \tag{19}$$

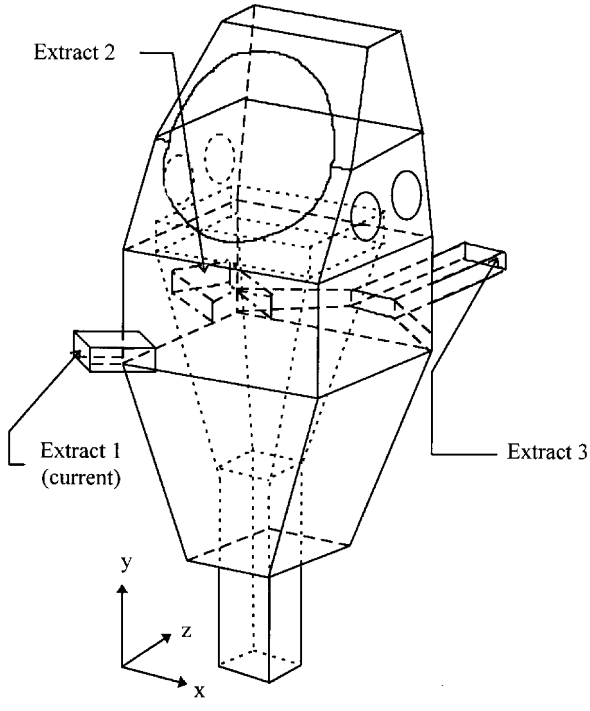

Figure 9. Locations of different extraction points.

Table 2. Fluid age calculations for specific zones within the isolator and for the scenario whereby all the glove ports are uncovered.

Extract position	Flow rate, kg s^{-1}	Turnover time, s	Mean fluid age, s					
			Outlet	Complete isolator	Ventilated Zone	Lower Rim Vents	Inner Hopper	Proposed Ventilated Zone
	0.115	17.87	17.17	37.54	25.20	46.67	83.35	13.98
	0.23	8.94	8.66	18.46	12.48	23.20	40.67	6.89
1	0.46	4.47	4.29	10.04	6.66	12.20	22.61	3.77
	0.69	2.98	2.86	6.94	4.65	8.47	15.43	2.66
	0.92	2.23	2.15	4.67	3.14	5.82	10.35	1.74
	0.115	17.87	17.56	20.35	11.70	18.04	52.45	8.39
	0.23	8.94	8.71	10.89	5.87	9.11	25.98	4.17
2	0.46	4.47	4.40	5.16	2.91	4.39	13.50	2.14
	0.69	2.98	2.92	3.38	1.95	3.02	8.70	1.39
	0.92	2.23	2.19	2.54	1.46	2.26	6.54	1.05
	0.115	17.87	17.65	19.41	10.69	15.99	51.78	7.92
	0.23	8.94	8.81	9.67	5.37	8.11	25.65	3.94
3	0.46	4.47	4.42	4.91	2.64	3.82	13.34	2.03
	0.69	2.98	2.94	3.23	1.79	2.68	8.85	1.32
	0.92	2.23	2.21	2.44	1.34	2.01	6.45	0.99
All glove ports	0.115	17.87	17.05	47.35	25.46	38.59	128.61	18.60
uncovered	0.23	8.94	8.55	23.82	12.75	19.30	64.89	9.34
(complete glove	0.46	4.47	4.28	12.06	6.41	9.66	33.03	4.71
failure)	0.69	2.98	2.85	8.14	4.29	6.45	22.42	3.17
	0.92	2.23	2.14	6.19	3.24	4.85	17.13	2.40

where

$$\bar{V}_N = \frac{\dot{V}}{A_f} \tag{20}$$

The k-ε model is generally used where Re_f is about 3.0×10^4 or greater. This model uses a logarithmic law to relate two dimensionless groups u^+ and y^+. The log-law is written:

$$u^+ = \frac{1}{\kappa}\ln(Ey^+) \tag{21}$$

where

$$u^+ = \frac{u}{u_\tau} \tag{22}$$

and

$$y^+ = \frac{\rho u_\tau y}{\mu} \tag{23}$$

For smooth walls, the values of κ and E are 0.4 and 9.8 respectfully. y^+ is the non-dimensional normal wall distance while the friction velocity u_τ is deduced from:

$$u_\tau = \left(\frac{\tau_w}{\rho}\right)^{\frac{1}{2}} \tag{24}$$

Where Re_f is significantly less than 3.0×10^4, the log-law is no longer valid and it is more accurate to use the low Reynolds number k-ε model. This model damps the eddy viscosity where the Reynolds number is low, and modifies the definition of epsilon so that it goes to zero at the walls. It assumes a linear variation of velocity near surfaces.

Equation (6) becomes:

$$\mu_T = C_\mu f_\mu \frac{\rho k^2}{\varepsilon} \tag{25}$$

where

$$f_\mu = \exp\left[\frac{-3.4}{(1 + R_T/50)^2}\right] \tag{26}$$

and

$$R_T = \frac{\rho k^2}{\mu\varepsilon} \tag{27}$$

This low Reynolds number model was used for the extraction rates of 0.23 kg s^{-1} and 0.115 kg s^{-1}.

To resolve accurately the effects in the viscous sublayers, where the shear rates may be considered constant and the flow is basically laminar regardless of the degree of turbulence possessed by the principal flow, the value of y^+ should be significantly less than five[15,22]. In this study, y^+ has been evaluated in CFD along a series of grid points adjacent to the wall surfaces within the isolator; for models using both the k-epsilon turbulence model and the low Reynolds number k-epsilon turbulence model. In all cases, it was found that y^+ was less than ~ 7.

The discrepancy with the required value may be attributed to the fact that the wall-adjacent cells are, in fact, too distant from the surface for an accurate y^+ assessment in the sublayer. This matter could be investigated further through a process of grid refinement close to the walls; whereupon values of y^+ considerably less than 7 would be found. As such, work is currently in hand to improve the value of y^+ using a finer grid. However, due to the complex nature of the block structure used for the CFD model of the isolator, this work is not reported in this particular paper.

Operational procedures in pharmaceuticals companies are subject to strict regulations which are rigidly enforced. Nonetheless, it is sensible in this study to consider exceptional circumstances in which it is conceivable that the isolator may be unknowingly operated under impaired conditions. Past experience has shown that the rubber gloves in the side glove ports have a tendency to suffer from wear and tear, and therefore have the potential to fail completely if not regularly monitored. With this in mind, the containment implications of a 'worst case' scenario involving four completely uncovered glove ports have been investigated.

Table 2 displays the mean fluid age data for the specific zones described above. The results were computed for the three different extraction positions as shown in Figure 9, and for the scenario whereby all four glove ports are uncovered. In all cases, the effects of five different flow rates ranging from 0.115 kg s^{-1} to 0.92 kg s^{-1} were analysed.

RESULTS

Figure 5 provides a good, global picture of the nature of the air flows within the isolator. The high velocities near to the base of the inlet hatch face are clearly evident, as are the strong flows in the narrow rim vents above the extract. The strength of the inward flows decreases higher up the hatch face and the flows near the top of the system are relatively weak. Although the air movement within the inner hopper is generally minimal, the figure shows that some of the fast incoming air has a tendency to 'swoop' down into the top part of the inner hopper and then rise back up over the back rim. CFD has also predicted little air flow in the lower regions of the rim vents.

Figure 6, which displays the predicted air flow field on the xz-plane at $y = 2.16$ m, generally compares well with the corresponding experimental data (Figure 2). The directional agreement is good indicating how the flows travel towards the rear of the isolator whilst turning towards the rim vents. Quantitatively, a large proportion of the numerical results show a discrepancy of less than 15% when compared to their associated experimental values. The general pattern of the v velocities (in the negative y direction) is similar to Figure 2, with the higher values near the hatch face.

In a similar manner Figure 7, which provides a profile of the predicted hatch face w-velocities, is comparable with Figure 3. The high inflows of greater than 2.0 m s^{-1} at the lower left corner of the face were correctly predicted by CFD, as was the low inflow region towards the top right corner. However, although the numerical data did support a reduction in flow velocity with height, this reduction was predicted as being more abrupt than that measured. The relatively strong circumferential flows were also found using CFD.

The fluid age prediction shown in Figure 8 supports the air flow model. Given that the air entering the hatch face is defined as having zero 'age', it is natural that in the region close to the face, the air is relatively 'young'. Where there is limited air motion however, such as within the inner hopper and the lower sections of the rim vents (below the extract), the fluid is stagnant and therefore 'old'. As mentioned above, only the top part of the inner hopper is well ventilated by the incoming air and this is highlighted by the results. The fluid ages at the base of the rectangular chute are relatively low since in this region some air is being pulled up from the reactor vessel into the isolator.

Figure 10 displays graphs that illustrate the predicted variation in IOIP (Indicator of Isolation Performance) and IOVP (Indicator of Ventilation Performance) with extraction flow rate and position. In addition to the complete isolator, Table 2 also presents the values for the mean fluid age in the particular locations within the device named previously: Ventilated Zone, Lower Rim Vents, Inner Hopper and Proposed Ventilated Zone.

For the normal operational characteristics of the system, IOIP1 = 0.313 and IOVP1 = 0.213 (Figure 10), suggesting both a lack of sufficient protective air flow at the face, and a relatively inefficient ventilation ability. Table 2 gives a value of 10.04 s for the mean fluid age of the whole system and, as expected from equation (12), the average 'age' at the outlet position, 4.29 s, compares favourably with the turnover time of 4.47 s. The 'Ventilated Zone' returns a value of 6.66 s for the mean 'age' whilst the 'Lower Rim Vents' have a value of 12.2 s. As it is shielded from the principal flows, the 'dead zone' of the inner hopper is a region of 'old' fluid where, on average, the 'age' is as high as 22.61 s.

From Figure 10, it is evident that the degree of isolation offered by the hatch face (IOIP1) is greatly influenced by the rate of air being extracted from the isolator. Doubling the flow rate to 0.92 kg s^{-1}, for example, results in a 180% increase in this indicator. Similarly, reducing the flow rate four fold to just 0.115 kg s^{-1} yields a dangerously low value of 0.07. Ventilation efficiency, though, remains largely independent of the flow rate suggesting that the degree of recirculative flows induced by turbulence is not governed by the rate of air extraction. Generally speaking, doubling the flow rate simply halves the turnover time, mean fluid age, outlet fluid age, and all the specific 'ages' analysed.

Moving the extract to the rear left corner of the isolator (extract position 2) appears to be beneficial in terms of both containment indicators. The value of IOVP (IOVP2) is improved by about 100% thus showing that ventilation efficiency is controlled by the relative positions of the inlet and outlet registers. The values in Table 2 emphasize this improvement showing that the mean fluid age for the complete isolator when extracting at 0.46 kg s^{-1} is reduced from 10.04 s to 5.16 s, whilst all the other specific 'ages' are also lowered by approximately 50%. Further, the isolation performance (IOIP2) is significantly increased for high flow rates indicating that this arrangement would be advantageous in terms of the protection offered to the operators working in the surrounding environment. At a flow rate of 0.92 kg s^{-1}, IOIP2 = 1.0 suggesting perfect, ideal flow conditions at the hatch face. The value of IOIP is marginally worse at low flow rates than the normal configuration; however, it is doubtful that these rates would ever be employed.

Figure 10 also shows that placing the extract centrally at the back of the isolator (extract position 3) yields a small additional improvement in the value of IOVP. For high flow rates, the degree of isolation performance is also increased further, whilst an IOIP value of unity is maintained for a flow rate of 0.92 kg s^{-1}.

The containment implications of having all four glove ports uncovered with the normal operational conditions in place (extract position 1) are significant. The majority of the specific fluid ages cited in Table 2 are increased, indicating a greater likelihood of particulate accumulation within the isolator. The ventilation performance (IOVP_P) is lowered by approximately 17%. At the same time, the isolation at the hatch face (IOIP_P) is substantially reduced over the whole range of flow rates; but particularly above 0.46 kg s^{-1} where the reduction is at least 50%.

DISCUSSION

The results show that the CFD predictions agree reasonably well with the *in-situ* measurements and there are several possible explanations for any discrepancies.

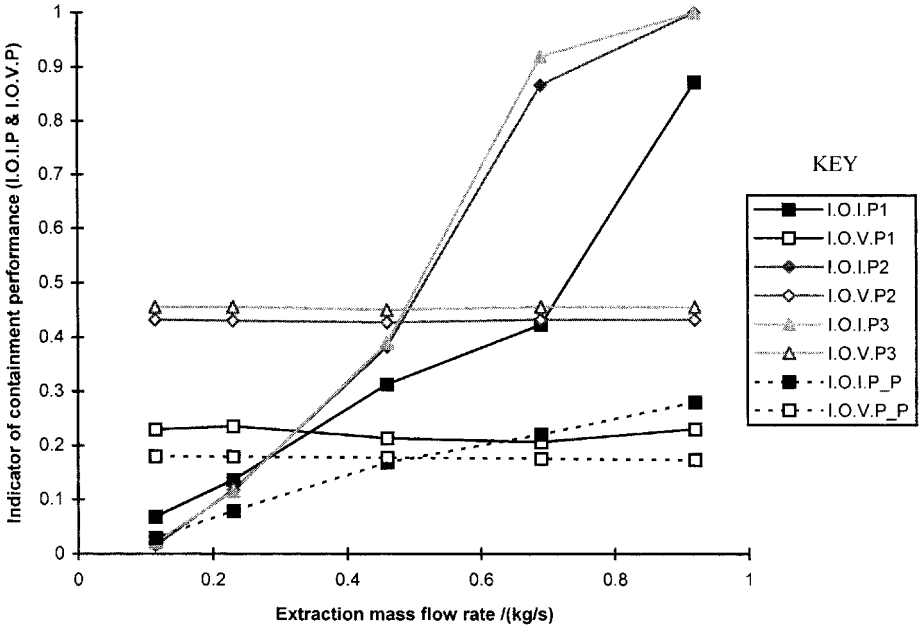

Figure 10. Graphs of the variations of two indicators of containment performance with extraction rate and extraction location.

In general, the validity of CFD predictions is compromised by the magnitude of the computational mesh, the accuracy of the hybrid differencing scheme in solving the complex non-linear fluid flow equations, and the selection of turbulence model to simulate the unsteady, random motion of the flow. For this study, we concluded that the solution was adequately grid independent, indicating that any further refinement of the grid would yield no significant differences in the results obtained.

However, the use of the hybrid differencing scheme probably induced numerical diffusion errors since the accuracy of the inherent Taylor series truncation error is only first order. This scheme is favoured due to its ability to produce realistic solutions, and its stability compared to higher order schemes. As computer hardware becomes more powerful, it will be possible to increase the accuracy of all solution schemes. In addition, although two turbulence models were employed—the *k*-epsilon model and the low Reynolds number *k*-epsilon model (depending on the Reynolds number at the hatch face)—these models erroneously assume that the turbulent viscosity is isotropic, i.e. that the ratio between Reynolds stress and mean rate of deformation is the same in all directions. No currently available turbulence model for commercial CFD codes is entirely accurate. However, the introduction of algebraic stress models that incorporate the effects of anisotropy into CFD simulations could improve solutions.

Furthermore, the accuracy of the CFD model generated to simulate the operational characteristics of the isolator is affected by a physical assumption that may well be incorrect. The air pressure at the hatch face was modelled as being constant across the whole face. In reality, however, it is highly likely that the pressure on this boundary is not constant. Air currents and obstacles in the work space surrounding the isolator will induce variations in the pressure at the face, and the air passing through the face in close proximity to the hatch rims will be influenced by viscous drag forces. The effect of the surrounding environment on the air flows in the isolator could be investigated by modelling the entire plant room. However, given that over 95,000 grid cells were used for the isolator alone, this course of action was considered impractical and unwarranted since it would require a huge amount of additional computer running time, and probably yield little difference in the overall results obtained.

There are also likely to be errors in the experimental data. It was very difficult to measure accurately the three-dimensional flow field due to the high degree of turbulence within the enclosure, the inevitable interference of the flow by the measuring equipment itself, and an inability to control the extract flow rate which had a tendency to fluctuate slightly. Furthermore, due to the fact that the isolator was needed for another period of manufacturing, it was not possible to repeat the experiments as often as perhaps was necessary, nor investigate the effects induced by changes in the operational characteristics of the system. Ideally, a scaled model of the isolator should be constructed and extensive tests conducted under controlled conditions in a laboratory. However, this would be both costly and time consuming.

The CFD predictions obtained indicate that, as it stands, the isolator may have an insufficiently strong flow field at the hatch face, and an inadequate ventilation characteristic. The relatively weak flows generated in certain regions of the face could provoke a leakage of contaminants into the room environment which, in turn, could pose a threat to personnel safety. Inefficient ventilation means that residual particulates have the potential to remain in the air space for undesirably long periods of time, and are more likely to deposit on surfaces thus creating a further health hazard.

Fluid age calculations were performed in particular locations to help understand what motivated a design involving two hoppers, one inside the other. The high 'ages' found in the inner hopper suggest a 'dead', stationary flow field and this is perhaps beneficial in allowing the bulk of the charging material to fall unhindered into the reactor vessel

below. If this region were well ventilated, material would be pulled up from within the inner hopper to be extracted out and lost on the filter. For this device, the ventilation system must deal solely with the residual particulates that are left in the top air space following the charging procedure. It must not interfere with the bulk material since this would naturally lead to a reduction in the manufacturing output. Incidentally, since there are often flammable solvents within the reactor vessel, extracting downwards into this vessel is unacceptable.

Unwanted, however, are the high 'ages' developed in the lower regions of the rim vents (between the two hoppers and below the extract). This zone should be well ventilated but, conversely, is likely to be the source of substantial particulate accumulation due to high fluid residence times. One possible modification to the current design, therefore, would involve eliminating this zone altogether. The comparatively low 'age' results computed in the 'Proposed Ventilated Zone' (Table 2) emphasize the improvements that such an action would bring to the ventilation efficiency within this important top section of the isolator.

Indicators of performance have highlighted the current deficiencies with the isolator and outlined the relative improvements brought about by changes to the extract flow rate and location. A centrally positioned rear extract could double the ventilation efficiency of the apparatus, and improve isolation performance over the majority of computed flow rates. The only problem with implementing such a solution appears to be the costs involved in relocating the extraction ducting, and developing more fan power. In addition, these CFD methods have enabled the detrimental effects of complete glove failure during the charging procedure to be established.

CONCLUSIONS

This study has highlighted the usefulness of numerical predictive techniques in the evaluation of the containment performance of an industrial ventilated enclosure. Due to manufacturing demands and extreme costs, it would simply not be practical to carry out extensive on-site experiments in order to investigate the benefits that would result from any modifications to the isolator's design. However, given that the CFD data have been significantly validated by both experimental results and certain theoretical formulations, it would appear that the use of a commercially available CFD code as a predictive tool for this work is justified. The current limitations of CFD have been discussed. With these in mind, the advantage of CFD clearly lies in its ability to accurately forecast the likely *trends* produced by a hydrodynamic system, rather than give extremely precise results at specific locations.

Two indicators of containment performance (IOIP and IOVP) have been defined in order to assist the management personnel at Zeneca in quantifying just how effective their device is. Although the ideal value for isolation performance is clearly obtainable, a value of unity for the IOVP is far beyond the reach of this particular device due to the very high fluid ages developed within the rim vents and the inner hopper. For this reason, the indicator of ventilation performance should be used as a quick and easy method for assessing *the proportional benefits* that would result from any change in the design of the apparatus, rather than as a tool that enables a direct comparison with the ideal ventilation scenario.

Relocating the extraction position at the rear of the isolator could lead to a 110% improvement in the ventilation performance of the apparatus, which is important if residual particulates are to be removed quickly and efficiently. In addition, extracting from this position at a flow rate of $0.92\,\mathrm{kg\,s^{-1}}$ is virtually guaranteed to establish a perpendicular flow of at least $0.5\ \mathrm{m\,s^{-1}}$ across the whole hatch face; thus satisfying the HSE guideline completely. These two changes seem viable for Zeneca to implement provided that the costs involved are not too high, disruption to manufacturing schedules is kept to a minimum, and the extra noise resulting from increased fan power is not intolerable.

The 'Indicator of Ventilation Performance' relied upon the computation of 'fluid age' which also proved to be a useful tool in establishing how the system was designed to operate, and how certain modifications to its topology could improve its effectiveness. The inner hopper appears to be suitably designed for ensuring that large amounts of charging material are not lost to the filtration system. Unfortunately, although the containment benefits that would result from eliminating the poorly ventilated 'Lower Rim Vents' are clearly evident, this would necessitate the design of an entirely new system which would be very expensive.

One further issue regarding safety is concerned with how wear and tear of the apparatus could lead to poor containment. This work has shown that a 'worst case' scenario involving complete glove failure during the charging procedure could have severe implications on personnel safety. Thus, the isolator analysed is not intrinsically safe but relies on good management procedures.

At Zeneca, every effort is made to ensure that current occupational health guidelines are rigidly followed and personnel are protected from any potentially harmful exposure to 'dust' contamination. As such, the company continually seeks to improve the containment performance of its systems and is always receptive to suggestions of how to do so. Having read this report, the management personnel at Zeneca will be considering the recommendations it highlights and, where appropriate, may use them to assist in the design of new, more effective containment devices.

Further work is currently being produced to help confirm the reported findings and validate the specific methods undertaken during the analysis. Particle tracking models are being developed to predict the likely routes of particles released within the isolator, and laboratory tests on ventilation efficiency and 'fluid age' are ongoing. At the moment, one of the problems associated with the isolator is that the air flow generated at the hatch face will draw unfiltered air into the charging system thus contaminating the manufactured product. Hence, a possible solution to prevent all cross-contamination that involves the supply of clean, filtered air from an overhead plenum plate is currently being modelled using CFD.

Finally, further investigations will soon commence into how the small electrical charges present on the individual particles comprising the charging material are likely to influence their movements within the isolator. Novel ways of ensuring better containment in industry will also be considered, such as the use of electrostatic forces within specifically designed enclosures.

NOMENCLATURE

A_f	area of the hatch face, m^2
C_μ, $C_{1\varepsilon}$, $C_{2\varepsilon}$	standard k-ε model turbulence constants
d_f	diameter of the hatch face, m
E	log-law constant
E_{ij}	mean rate of fluid deformation tensor
f_μ	low Reynolds number function
g	acceleration due to gravity, ms^{-2}
H	specific enthalpy, $kJkg^{-1}$
k	turbulent kinetic energy, m^2s^{-2}
P	pressure, Pa
Re_f	Reynolds number at the hatch face
R_T	local turbulent Reynolds number
S	source or sink term
T	temperature, K
t_a	fluid age, s
t_m	volume averaged mean fluid age, s
t_o	volume averaged mean fluid age at extract, s
U	(u, v, w) velocity, ms^{-1}
u	velocity component in the x direction, ms^{-1}
u^+	dimensionless group
u_τ	friction velocity, ms^{-1}
V	volume, m^3
$\dot{V}$	volume flow rate, m^3s^{-1}
V_N	'face' velocity normal to the hatch face, ms^{-1}
$\bar{V}_N$	mean face velocity, ms^{-1}
V_{P1}	velocity parallel to hatch face (vertically), ms^{-1}
V_{P2}	velocity parallel to hatch face (horizontally), ms^{-1}
v	velocity component in the y direction, ms^{-1}
w	velocity component in the z direction, ms^{-1}
y^+	dimensionless normal wall distance

Greek symbols

Γ	diffusion coefficient, $kgm^{-1}s^{-1}$
Γ_x	diffusion coefficient in the x direction, $kgm^{-1}s^{-1}$
Γ_y	diffusion coefficient in the y direction, $kgm^{-1}s^{-1}$
Γ_z	diffusion coefficient in the z direction, $kgm^{-1}s^{-1}$
ε	energy dissipation rate, m^2s^{-3}
θ	angle of the hatch face to the horizontal xz-plane, degrees
κ	log-law constant
λ	thermal conductivity, $kWm^{-1}K^{-1}$
μ	dynamic viscosity, $kgm^{-1}s^{-1}$
μ_{eff}	effective viscosity, $kgm^{-1}s^{-1}$
μ_T	turbulent viscosity, $kgm^{-1}s^{-1}$
ρ	density, kgm^{-3}
σ_k, σ_ε	standard k-ε model turbulence constants
τ	nominal time constant, s
τ_w	shear stress at the wall, $kgm^{-1}s^{-2}$
φ	general variable

Abbreviations

CFD	computational fluid dynamics
FTS	false time step
HEPA	high efficiency particulate air
HSE	Health and Safety Executive
IOIP	'Indicator of Isolation Performance'
IOVP	'Indicator of Ventilation Performance'
OEL	operator exposure limit

REFERENCES

1. Rumer, R. R. and Ryan, M. E., 1995, *Barrier Containment Technologies for Environmental Remediation Applications* (Wiley).
2. McDermott, H. J., 1976, *Handbook of Ventilation for Contaminant Control (including OSHA requirements)* (Ann Arbor Science Publishers).
3. Quarini, G. L., Chang, Y. C., Tierney, M. J. and Poulter. R., 1997, Characteristics and 'figures of merit' for the value of the ventilation in clean rooms, *Trans IChemE, Part A, Chem Eng Res Des*, 75: 672–676.
4. Mackler, S. E, 1996, Current issues in the design and production facilities for cell and gene therapy, *Genetic Engineering News*, 16 (12).
5. Hill, D. and Beatrice, M., 1991, Facility requirements for biotech plants, *J of Parenteral Science and Technology*, 45 (3): 132–137.
6. Rahe, H., 1996, Hierachy of containment technologies, Clean Rooms '96 Proceedings (International Society for Pharmaceutical Engineering (ISPE)).
7. Typical performance range of various containment devices, *Product Brochure: Containment Solutions for the Pharmaceutical and Chemical Industry*, 1997 (Extract Technology).
8. Hu, P., Ingham, D. B. and Wen, X., 1996, Effect of the location of the exhaust duct, an exterior obstruction and handle on the air flow inside and around a fume cupboard, *Ann Occup Hyg*, 40 (2): 127–144.
9. Özdemir, I. B., Whitelaw, J. H. and Biçen, A. F., 1993, Flow structures and their relevance to passive scalar transport in fume cupboards, *Proc IMechE, Part C, J of Mechanical Engineering Science*, 207: 103–115.
10. Agutter, P. A., Buss, A. D., Noble, M., Titchener-Hooker, N. J. and Turner, M. K., 1996, Computational fluid dynamics as a tool in biosafety to assess the release of microorganisms from a bioprocess, *Proc of the Third CFX International Users Conference*, 371–375.
11. HSE, 1991, *Dust: General Principles of Protection, Guidance Note EH44*, ISBN 0 11 885596 6 (HMSO).
12. Sandberg, M. and Sjöberg, M., 1983, The use of moments for assessing air quality in ventilated rooms, *Building and Environment*, 18 (4): 181–197.
13. Sandberg, M., 1983, Ventilation efficiency as a guide to design, *ASHRAE*, 89: 455–479.
14. Özdemir, I. B., Whitelaw, J. H. and Biçen, A. F., 1996, Flow properties and passive scalar transport in a model room with relevance to ventilation efficiency, *Trans IMechE*, 210: 297–307.
15. Versteeg, H. K. and Malalasekera, W., 1995, *An Introduction to Computational Fluid Dynamics: The Finite Volume Method* (Addison Wesley Longman Limited).
16. Spalding, D. B., 1972, A novel finite difference formulation for differential expressions involving both first and second derivatives, *Int J Num Meth Eng*, 4: 551–559.
17. Rhie, C. M., 1981, A numerical study of the flow past an isolated airfoil with separation, *PhD Thesis* (Department of Mechanical and Industrial Engineering, University of Illinois at Urbana-Champaign).
18. Rhie, C. M. and Chow, W. L., 1983, Numerical study of the turbulent flow past an airfoil with trailing edge separation, *AIAA J*, 21: 1527–1532.
19. Van Doormal, J. P. and Raithby, G. D., 1984, Enhancements of the SIMPLE method for predicting incompressible fluid flows, *Numer Heat Transfer*, 7: 147–163.
20. AEA Technology, 1997, *CFX-4.2: Solver*.
21. Danckwerts, P. V., 1995, Continuous flow systems. Distribution of residence times, *Chem Eng Sci*, 50: 3857–3866.
22. Massey, B. S., 1989, *Mechanics of Fluids* (Chapman & Hall).

ACKNOWLEDGEMENTS

This work was jointly funded by MAFF (Ministry of Agriculture, Food and Fisheries) and Zeneca Pharmaceuticals. In particular, we should like to thank the senior staff at Zeneca for their help in producing this paper.

ADDRESS

Correspondence concerning this paper should be addressed to Dr J. M. Reglar, Department of Mechanical Engineering, Room 1.16, Queen's Building, University of Bristol, Bristol BS8 1TR, UK.

The manuscript was received 30 July 1998 and accepted for publication after revision 22 October 1998.